



# Development of the real-time double-ring fusion neutron time-of-flight spectrometer system at HL-2M

Bo-Wen Zheng<sup>1,2</sup> · Wei Zhang<sup>1,2</sup> · Tong-Yu Wu<sup>1,2</sup> · Si-Cheng Huang<sup>1,2</sup> · Yi-Po Zhang<sup>3</sup> · Xiu-Feng Xu<sup>1,2</sup> · Shi-Biao Tang<sup>1,2</sup> · Ze-Jie Yin<sup>1,2</sup>

Received: 3 September 2019 / Revised: 8 October 2019 / Accepted: 13 October 2019 / Published online: 14 November 2019  
© China Science Publishing & Media Ltd. (Science Press), Shanghai Institute of Applied Physics, the Chinese Academy of Sciences, Chinese Nuclear Society and Springer Nature Singapore Pte Ltd. 2019

**Abstract** A real-time double-ring neutron time-of-flight (TOFII) spectrometer system has been proposed to achieve plasma diagnosis on HL-2M tokamak with a relatively high count rate and sufficient energy resolution. The TOFII system is in its development stage, and this work describes its characteristics in terms of design principle, system structure, electronic system design, preliminary tests, and neutron transport simulation. The preliminary test results illustrate that the TOFII system can demonstrate the real-time dynamic spectrum every 10 ms. The results also show that based on the support vector machine method, the  $n$ - $\gamma$  discrimination algorithm achieves the discrimination accuracy of 99.1% with a figure of merit of 1.30, and the intrinsic timing resolution of the system is within 0.3%. The simulated flight time spectrums from 1 to 5 MeV are obtained through the Monte Carlo tool Geant4, which also provide the reasonable results. The TOFII system will then be calibrated on mono-energetic neutron sources for further verification.

**Keywords** Time-of-light · Neutron spectrometer · Geant4 · HL-2M

## 1 Introduction

The neutron measurements and diagnostics are essential and reliable around many fusion devices, for their capability of carrying parameters about the condition of plasma in the deuterium–deuterium (D–D) and deuterium–tritium (D–T) fusion reactions. The detailed information regarding the intensity and motional state of the fuel ions, tritons, and deuterons could be obtained from the neutron emission spectroscopy (NES) [1]. The time-of-flight (TOF) technique has been utilized for years in many tokamak facilities worldwide, such as JT-60U [2], JET [3], and CERN [4], as a means to achieve the high count rate and sufficient energy resolution of NES diagnosis of D–D reaction [5, 6]. The HL-2M [7–9], which is the modification of the first large controlled fusion experimental device in China (HL-2A) [10–12], is expected to be stable and flexible in experiments of high-performance plasma physics, techniques, and engineering toward ITER and fusion reactor [7]. Therefore, a novel TOFII spectrometer is proposed to achieve advanced 2.45 MeV NES diagnostics at HL-2M.

The TOF spectrometer [13, 14] is based on the neutron elastic scattering inside the plastic scintillators, and Fig. 1 illustrates the principle of the TOF technique. A fraction of the collimated incident neutrons ( $n$ ) is scattered in the S1 plastic scintillator detector. As a result of this, recoil protons ( $p_r$ ) and scattered neutrons ( $n_s$ ) are produced from the elastic scattering between the incident neutrons and the hydrogen nuclei ( $p_H$ ) in S1:  $n + p_H \rightarrow n_s + p_r$ . After the flight path of  $L$ , a fraction of the scattered neutrons is

---

This work was partially supported by the National Science and Technology Major Project of Ministry of Science and Technology of China (Nos. 2014GB109003 and 2015GB111002) and the National Natural Science Foundation of China (Nos. 11375195, 11575184, 11375004, and 11775068).

---

✉ Bo-Wen Zheng  
myzbw@mail.ustc.edu.cn

<sup>1</sup> State Key Laboratory of Particle Detection and Electronics, University of Science and Technology of China, Hefei 230026, China

<sup>2</sup> Department of Modern Physics, University of Science and Technology of China, Hefei 230026, China

<sup>3</sup> Southwestern Institute of Physics, Chengdu 610041, China

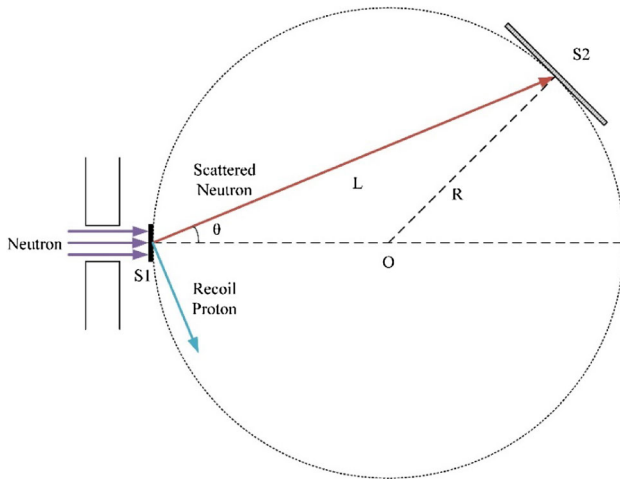


**Fig. 1** Schematics of the TOF technique. The S1 and S2 scintillators are placed tangentially on a constant TOF sphere with center O

recorded in the S2 plastic scintillator detector similar to the scattering in S1. Consequently, an incident neutron is successively recorded by a pair of signals produced in S1 and S2 detectors. The middle points in the mid-planes of S1 and S2 detectors are placed tangentially on a constant TOF sphere with a radius of  $R$ , and the scattering angle of neutrons reacted in S1 is  $\theta$ . Based on the neutron elastic scattering in S1 and the geometrical structure of the TOF sphere in Fig. 1, the scattered neutron energy  $E_S$ , the flight path of  $L$ , and the flight time  $t_f$  of the scattered neutrons are specified in Eqs. (1)–(3) [14, 15]:

$$E_S = E_n \cdot \cos^2 \theta, \tag{1}$$

$$L = 2R \cdot \cos \theta, \tag{2}$$

$$t_f = 2R \left( \frac{m}{2E_n} \right)^{1/2}, \tag{3}$$

where  $E_n$  is the energy of incident neutrons and  $m$  is the neutron mass. As shown in Eq. (3), for a constant TOF sphere, the flight time  $t_f$  is independent of the scattering angle  $\theta$  and is only influenced by the incident neutron energy  $E_n$ . Therefore, with the precise measurement of  $t_f$ , the incident neutron energy spectrum can be derived from the measured  $t_f$  spectrum. As long as the neutron is single scattered by hydrogen in S1 and is recorded in S2 by its first scattering [5], the relationship between  $E_n$  and  $t_f$  remains the same.

In this work, a novel real-time TOFII spectrometer is proposed and described to achieve NES diagnosis of D–D reaction on HL-2M with a high count rate and sufficient energy resolution. The overall design of the TOFII, the implementation, and the preliminary test results of the spectrometer are all introduced. The neutron transportation simulation of the TOFII spectrometer has been performed

with Geant4 [16], and the simulation provides positive results to the design of the TOFII system.

## 2 Overall design of the TOFII spectrometer system

The traditional design of the TOF spectrometer as shown in Fig. 1 has been performed on fusion devices for years [1, 2]. However, increasing the length of S2 to improve the number of detected neutrons can degrade the resolution of the  $t_f$  spectrum. As a result, the requirements on efficiency and energy resolution of the TOF spectrometer conflict against each other [1]. In order to balance the contradictory requirements of the efficiency and energy resolution, the TOFII spectrometer is proposed for NES diagnosis of the D–D reaction on HL-2M. Figure 2 demonstrates the structure of the TOFII techniques. Compared with the traditional TOF design in Fig. 1, distinct improvements of the S2 detectors can be found in TOFII. Instead of utilizing a long S2 detector for high efficiency, the S2 in the TOFII spectrometer is split into two rings of shorter plastic scintillators ( $S2_a$  and  $S2_b$  in Fig. 2) tangential to the TOF sphere (radius  $R = 1000$  mm). This change of S2 decreases the deviation between the S2 and the sphere, which leads to higher resolution. Then, the  $S2_a$  and  $S2_b$  detectors are both tilted away from the TOF sphere (angle  $\alpha$  in Fig. 2) to improve the time uncertainty caused

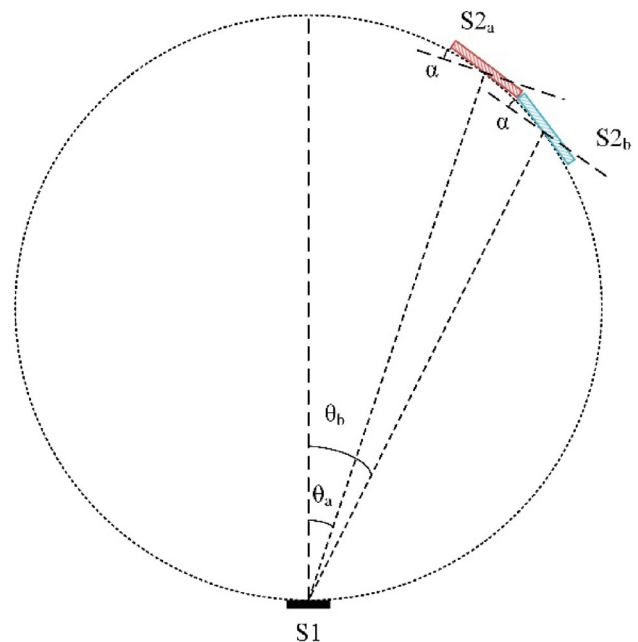


**Fig. 2** The structure of the TOFII techniques. The  $\theta$ ,  $\theta_a$ , and  $\theta_b$  are the scattering angles of the incident neutron;  $\alpha$  is the tilting angle to middle points of the  $S2_a$  and  $S2_b$  detectors

**Table 1** Dimensions of S2 trapezoidal scintillators in TOFII given as top width ( $w_1$ ), base width ( $w_2$ ), length, thickness, range of scattering angles ( $\theta_a$  and  $\theta_b$ ), and tilting angle ( $\alpha$ )

$w_1$ (mm)	$w_2$ (mm)	Length (mm)	Thickness (mm)	$\theta_a$	$\theta_b$	$\alpha$
70	100	280	17	22°–30°	30°–38°	3°

by the different light propagation time in  $S2_a$  and  $S2_b$  [1, 3].

The detailed information of TOFII is described here. The S1 consists of five layers of thin plastic scintillators, and each is equipped with two photomultiplier (PM) tubes. The above structure of S1 has considered the following three main reasons. Firstly, the S1 needs to be thick enough to ensure high neutron scattering rates [3]. Secondly, the PM tubes must be prevented from running into saturation with high event rates [1]. Thirdly, the time resolution of the photon signals in single plastic scintillator tends to perform poorly with the increase in the scintillator thickness [17]. Each layer of the S1 detector is a circular cylinder scintillator (model EJ-299-33, Eljen Technology) with a diameter of 50 mm and thickness of 6 mm. The scintillator is bonded to a polymethyl methacrylate (PMMA) light guide via silicone optical grease (model EJ-550, Eljen Technology), and it is then connected to two PM tubes (model R1828-01, Hamamatsu Photonics). The  $S2_a$  and  $S2_b$  consist of two rings of eighty trapezoidal scintillators (model EJ-200, Eljen Technology). Each scintillator is attached with a fish tail shape PMMA light guide and a PM tube. Table 1 summarizes the dimensions of the S2 scintillators in Fig. 2. Based on the dimensions of the S1 and S2 scintillator array, the scattering angle range for single S2 ring is  $\pm 4^\circ$  in TOFII, and this range is  $\pm 7^\circ$  in the traditional single ring TOFOR [5]. Consequently, the TOFII not only provides a higher geometrical energy resolution of 3.3% (2.45 MeV) than the single ring TOF design [1], but also has 1.19 times S2 detection area [1]. Each PM tube in the TOFII is fixed in a magnetically shielded soft-iron pipe, and the surfaces of all the scintillators and light guides are wrapped in aluminum foil and black vinyl for light tightness [1]. Figure 3 demonstrates the 3D representation of the scintillator array of the TOFII spectrometer.

The TOFII spectrometer system consists of several different parts, including the S1 and S2 scintillator array and four front-end electronics signal conditioning modules. It also has a data acquisition and processing (DAQ) board based on field-programmable gate array (FPGA) and PXI bus [18], as well as the software system on a host computer. Figure 4 illustrates the structure of the TOFII system. The collimated neutrons are first detected by the S1 and S2 scintillator array; the S1 and S2 signals from the PM tubes are sent to the ten-channel (S1) and thirty-

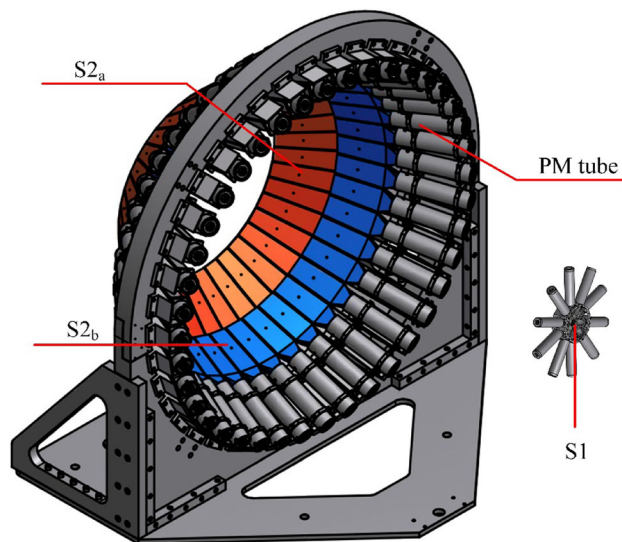


**Fig. 3** (Color online) 3D model of the S1 and S2 scintillator array of TOFII spectrometer at HL-2M. The S1 and S2 scintillators are placed on the same constant TOF sphere based on Fig. 2

channel (S2) front-end electronics signal conditioning modules for preprocessing. Then, the processed signals are collected by the DAQ board to achieve the neutron–gamma ( $n-\gamma$ ) discrimination and the  $t_f$  spectrum and pulse height spectrum calculation. Finally, the calculated spectra are uploaded to the software system for real-time display. After laboratory tests utilizing the programmable pulse generator (model AFG3251, Tektronix) and  $^{241}\text{Am}$ –Be source, the TOFII system can refresh the dynamic spectrum every 10 ms, and its count rate limit is 1 MHz. The scintillator array and its support frame are located inside a shield of polyethylene and lead. The shield also includes a cylindrical collimator with a length of 1.8 m and diameter of 50 mm. This is done as a means to avoid background neutrons in the experiment hall having influences on the  $t_f$  spectrum and provide collimated incident neutrons to the S1 scintillators.

### 3 System implementation

#### 3.1 Front-end electronics signal conditioning modules

Considering the finite area of the DAQ board, the front-end electronics signal conditioning modules are proposed

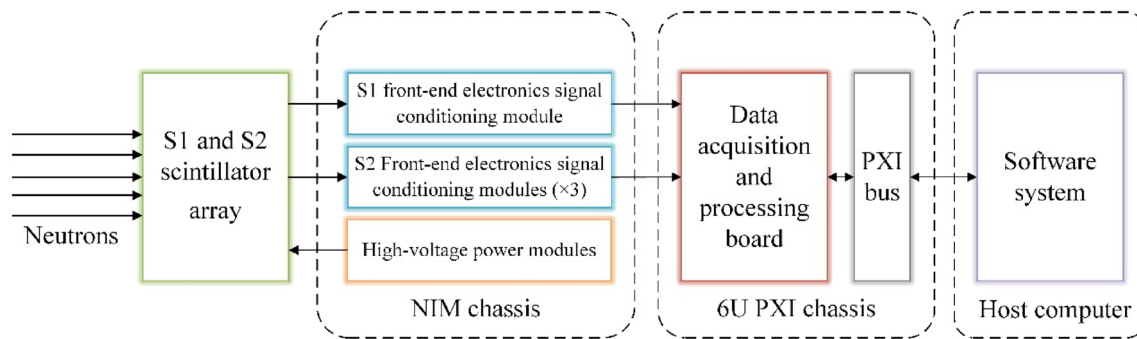


**Fig. 4** Schematic diagram of the TOFII system structure

to preprocess the analog signals from the PM tubes of the S1 and S2 scintillator array. The signal preprocessing includes impedance matching, analog-to-digital converter (ADC) driving, and amplitude discrimination. Figure 5 demonstrates the structure of the conditioning modules, meanwhile the S1 and S2 signal preprocessing procedures are described here. First, the output signal of each PM tube attached to the five layers of S1 requires a  $50\ \Omega$  resistance for impedance matching in order to avoid signal reflection. Then, the ten-channel S1 signals are summed [1] and split into two, one is sent to the ADC driving circuit to satisfy the differential input requirement of ADC in the DAQ board, the other is sent to the high-speed comparator to accomplish signal amplitude discrimination. Moreover, the low-voltage differential signaling (LVDS) output of the comparator is sent to the high-performance time-to-digital converter (HPTDC) in the DAQ board for time measurement. In the meantime, the eighty S2 output signals are fed into three, thirty-channel S2 conditioning modules, and

each channel signal is processed separately. Similar to the S1 conditioning module, the signal in each S2 channel is conditioned through impedance matching and amplitude adjustment. This is achieved by using a  $50\ \Omega$  resistance and an amplifier, respectively. The output of the amplifier is fed into the high-speed comparator for amplitude discrimination and further time measurement. The threshold values used in the comparators are determined by the software and sent to the front-end modules through the DAQ board. Notably, the output signals of the conditioning modules are sent to the DAQ board through 68-pin SCSI cables, to minimize crosstalk during the signal transmission.

### 3.2 Data acquisition and processing board

The DAQ board is designed as a standard PXI-6U peripheral equipment, consisting of the waveform digitization module, the time measurement module, the clock distribution module, the FPGA core processing unit, the

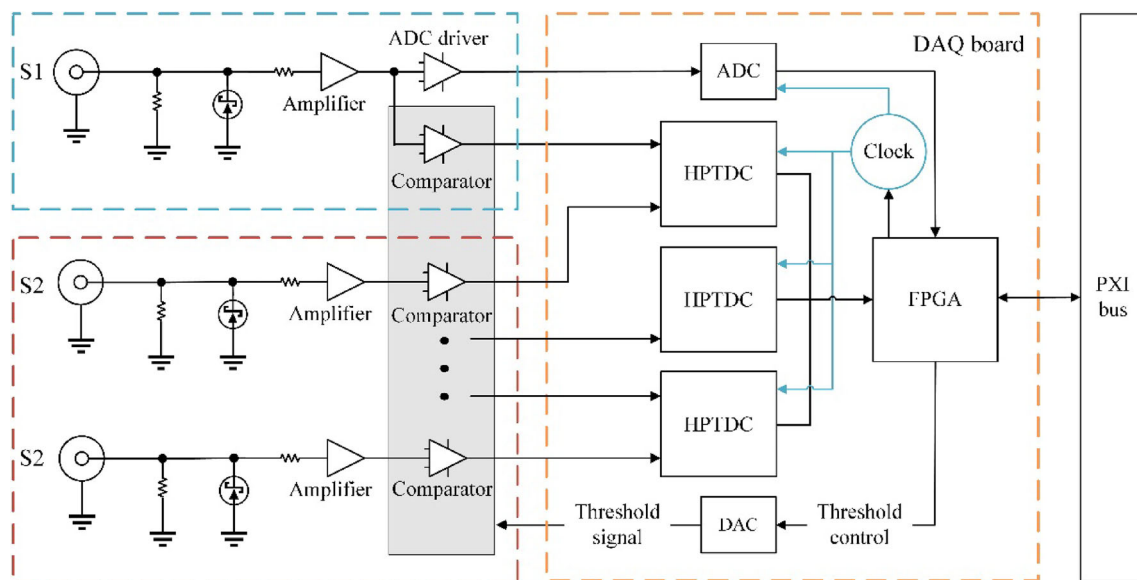


**Fig. 5** Structure of the front-end signal conditioning modules and the DAQ board for TOFII. The dashed frames on the left side illustrate the S1 and S2 front-end signal conditioning modules. The dashed frame on the right side describes the DAQ board

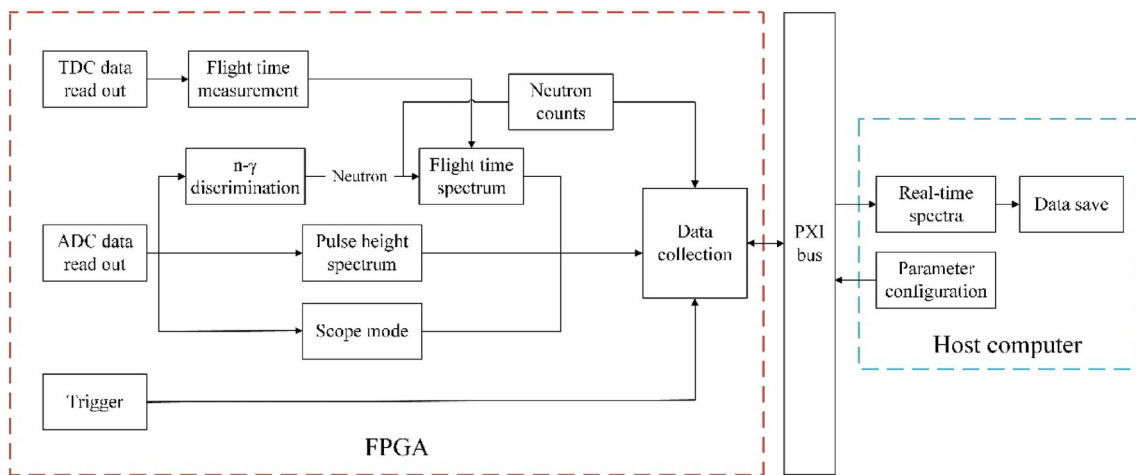


Fig. 6 Schematic diagram of the data flow and data processing procedure in the FPGA and host computer

bus interface module, and the threshold control module. Figure 5 illustrates the structure of the DAQ board. The S1 signal from the ADC driver in the front-end conditioning module is fed into the ADC for sampling to obtain the digital pulse information. Meanwhile, the S1 and S2 signals from the comparators are fed into three high HPTDC [19] to obtain the digital flight time information. Then, the digital information of pulse and flight time is sent to the FPGA to achieve the  $n-\gamma$  discrimination, pulse height spectrum measurement, and  $t_f$  spectrum measurement. In order to provide the analog threshold value to the comparators, the threshold signal from the FPGA is converted by the digital-to-analog converter (DAC) and sent to the front-end modules. The clock distribution for ADC is accomplished by using the AD9520 clock generator, and the clock for three HPTDC is provided by the SY89847 fan-out chip. All of the data communication between the DAQ board and the host computer is achieved through the PXI bus.

### 3.3 FPGA processing

In terms of the core processing unit, we choose the high-performance FPGA (Xilinx Kintex-7) to fulfill the real-time algorithm, the system control, and the data communication with the host computer [20] due to its flexible

programming, real-time parallel, and pipeline process capabilities [6, 20]. Figure 6 depicts the data flow and the data processing procedure in the FPGA. The measured result of HPTDC is read out to obtain the  $t_f$  value, and the ADC output is fed into the  $n-\gamma$  discrimination algorithm to distinguish the particle. Then, the  $t_f$  value will be used to construct the spectrum if it is the flight time of neutron. Meanwhile, the  $n-\gamma$  discrimination algorithm also provides the neutron counts in the selected time. Based on the ADC output data, the pulse height spectrum is calculated to illustrate the recoil energy and to ensure the wanted events are detected during the measurement process [1]. For the convenience of testing and operation, the scope mode is designed to display the real-time pulse waveform using the ADC sampling data. The results of neutron counts,  $t_f$  spectrum, pulse height spectrum, and scope mode waveform are collected and uploaded to the host computer through the PXI bus. Taking the time cost of the algorithm into account, the host computer is able to update the real-time spectrum every 10 ms, which has real-time characteristics compared with reconstructing the spectrum post-discharge [21]. The entire system is controlled by the external trigger pulse uploaded through the PXI bus.

Considering the intense gamma background in the HL-2M experiment hall [6], the EJ-299-33 plastic scintillator with excellent pulse-shape discrimination (PSD) capability

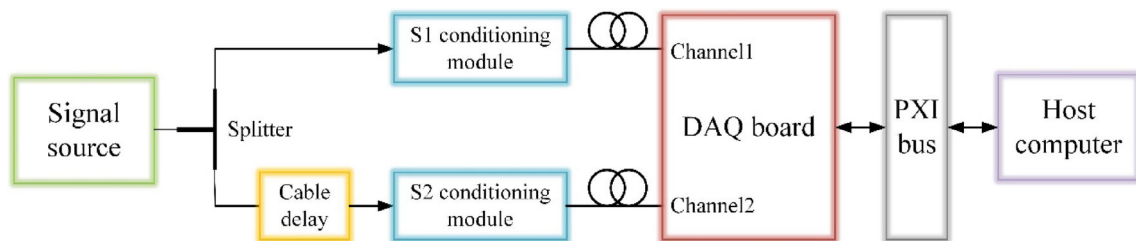
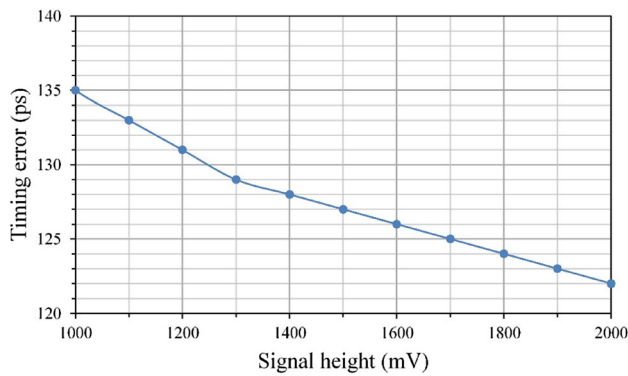


Fig. 7 Setup for the cable delay test to determine the intrinsic timing error



**Fig. 8** Timing error measured by using input pulse signals with the different heights from 1 to 2 V in step of 100 mV

[22, 23] is chosen for the TOFII system for  $n-\gamma$  discrimination. Instead of implementing the discrimination in software for post-processing or using the common pulse gradient analysis (PGA) algorithm [24, 25], we proposed the novel  $n-\gamma$  discriminate algorithm based on the SVM method [26–28]. This is utilized as a means to achieve the ultra-low delay and high accuracy of the real-time discrimination. Our previous experiment results of the SVM algorithm obtained by using the  $^{241}\text{Am-Be}$  source [6] demonstrates that the SVM method achieves discrimination accuracy of 99.1% with a FOM of 1.30, while the accuracy of the traditional PGA method is 92.1%. Meanwhile, the real-time pipeline process feature of the FPGA assures 250 million classifications per second, which is faster than most existing classifiers [6].

**Table 2** Physical models selected for neutron transportation in Geant4 simulation for TOFII

Physical process	Energy range	Physical model
Elastic scattering	< 4 eV	G4NeutronHPThermalScattering
	4 eV–20 MeV	G4NeutronHPElastic
	> 20 MeV	G4HadronElasticCHIPS
Inelastic scattering	< 20 MeV	G4NeutronHPInelastic
	> 20 MeV	G4BinaryCascade
Neutron capture	< 20 MeV	G4NeutronHPCapture
	> 20 MeV	G4NeutronRedCapture
Neutron fission	< 20 MeV	G4NeutronHPFission
	> 20 MeV	G4LFission

**Fig. 9** (Color online) Simulated TOFII  $t_f$  spectrum responses. The  $t_f$  spectrum is considered as a function of the neutron energy in the range 1–5 MeV

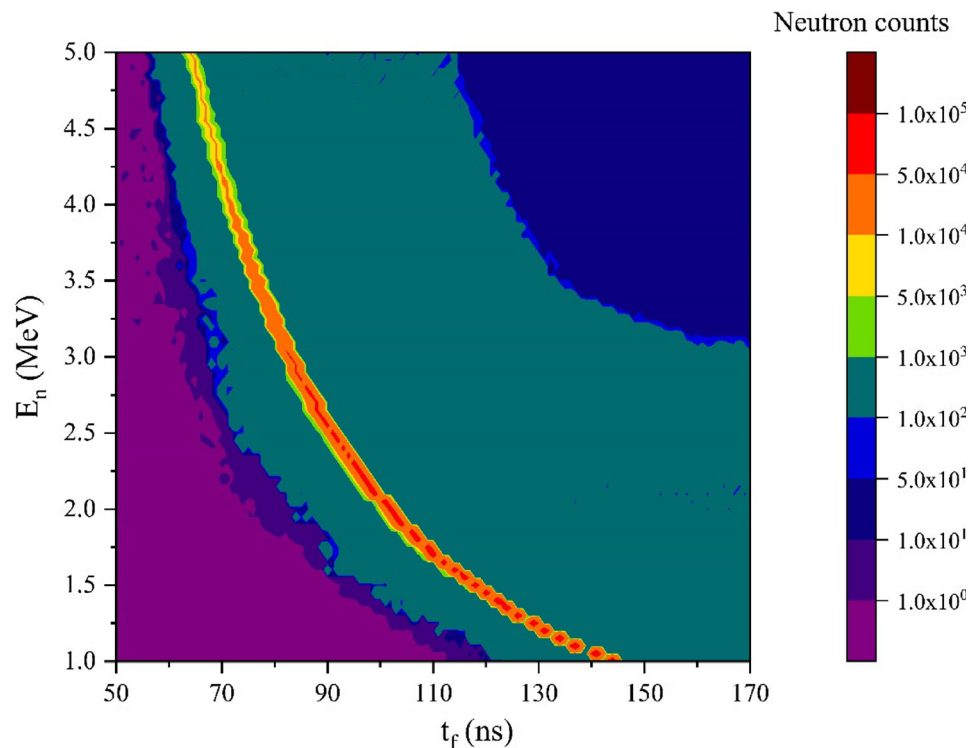
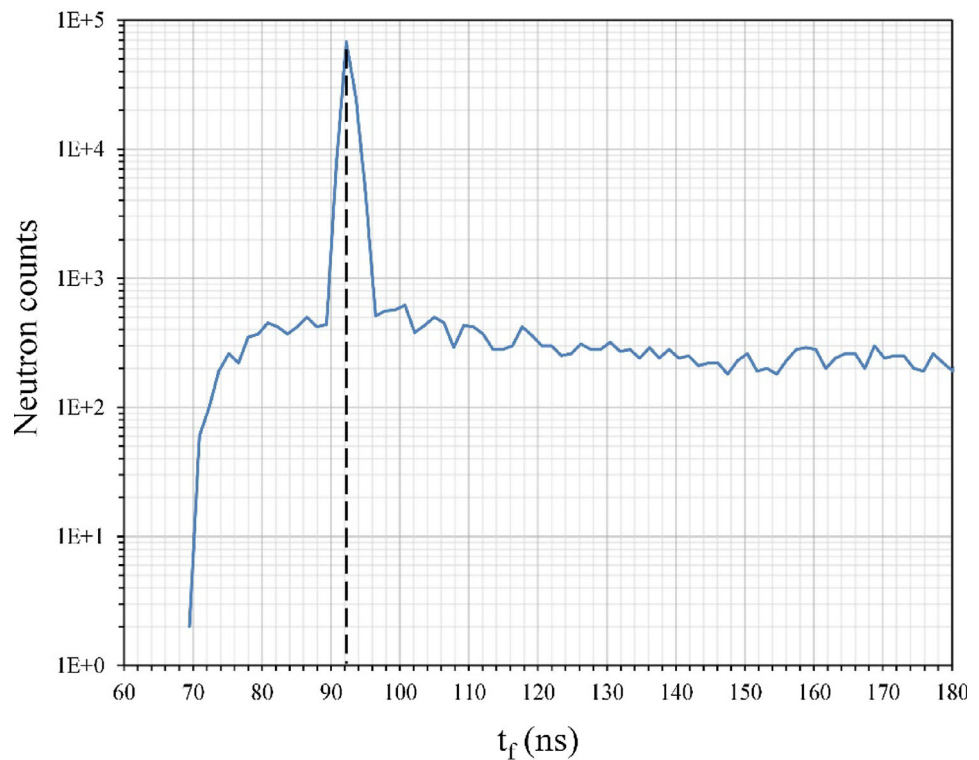


**Fig. 10** Simulated TOFII  $t_f$  spectrum for 2.45 MeV neutrons. The dashed line shows the peak value



The intrinsic timing error is a significant indicator of the TOFII spectrometer, which directly influences the resolution of the  $t_f$  spectrum. Therefore, the cable delay test has been used to determine the timing error [29]. As demonstrated in Fig. 7, the signal source is fanned into two channels of the S1 and S2 front-end signal conditioning modules, and the fixed delay line between these two channels is 5 m. As for the fixed time delay caused by the delay line, the standard deviation of the distribution of the measured time provides the intrinsic timing error of the system. By adjusting the input pulse signal height from 1 to 2 V in step of 100 mV (which is the pulse height range of the PM tubes), the measured timing error (RMS) [30] ranges from 135 ps to 122 ps, which results in a contribution of 0.3% to the resolution of the  $t_f$  spectrum. Figure 8 illustrates the timing error of the different input signal heights.

#### 4 Simulation of the flight time spectrum

As the HL-2M is still under construction in the Southwestern Institution of Physics [9], the Monte Carlo tool Geant4 is utilized to simulate and evaluate the TOFII performance. The Geant4 version 10.00.p01 provides a flexible combination of various physics models to assigned particles. The models and particles are defined by the user to describe the physical processes of the particle in the

interested material. Table 2 lists the physical models chosen in this work [31]. The neutron transport models change distinctly at 20 MeV, and the G4NeutronHP package provides high-precision models based on ENDF/B-VI library for neutrons below 20 MeV [32]. The TOFII geometrical structure is established according to Fig. 3, and the dimensions of S1 and S2 scintillator array are implemented within the simulation according to the description in Sect. 2. The density and H/C atomic ratio of S1 scintillator are 1.096 g/cm<sup>3</sup> and 0.927:1, respectively, and S2 scintillator results are 1.023 g/cm<sup>3</sup> and 1.102:1. Finally, we allow a mono-energetic uniform parallel neutron beam to collide with the S1 scintillator along its central axis in the energy range 1–5 MeV in step length of 50 keV, and Fig. 9 provides the  $t_f$  spectrum responses.

As observed in Fig. 9, the  $t_f$  spectrum peak values gradually decrease as the incident neutron energy increases, which agrees with Eq. (3). This pure geometrical response of TOFII to incident neutrons of different energies in Fig. 9 provides us with important information about the future  $t_f$  spectrum. In order to describe the spectrum information clearly, Fig. 10 shows the simulated  $t_f$  spectrum of 2.45 MeV neutrons in Fig. 9. Firstly, the broadening of the  $t_f$  peak is caused by the deviation between the S2 scintillators and the sphere of the TOFII spectrometer. Secondly, the spectrums have tails on both sides of the  $t_f$  peak [5], because of the neutron multiple scattering in the scintillators [21]. Thirdly, the neutron counts of the  $t_f$  spectrums in Fig. 9 tend to decline with the incident

neutron energy increases. This is due to the higher interaction cross section in the scintillators at lower neutron energies [1]. It is observed from Fig. 10 that the  $t_f$  peak value of 2.45 MeV neutron is around 92 ns, which is in accordance with the 65 ns flight time of the D–D neutron at JET after taking the difference of the TOF sphere radius into account (the radius of the TOF sphere at JET is 705 mm) [5]. The distribution of the  $t_f$  spectrums and the structure of the 2.45 MeV  $t_f$  spectrum are both similar to that of other TOF spectrometer in the published literature [1, 5]. The preliminary simulation results prove the practicability of the TOFII design, and the performance of TOFII should be further validated on mono-energetic neutron sources and the future built HL-2M.

## 5 Conclusion

The TOFII spectrometer system is designed to achieve NES diagnosis of the 2.45 MeV D–D reaction at HL-2M and has been described in terms of its system structure, electronic system design, and Monte Carlo simulation results. By using the double-ring scintillator array, the TOFII is able to concurrently balance the requirements of energy resolution and efficiency, which leads to a geometrical energy resolution of 3.3%. The electronic system of the TOFII realizes real-time data acquisition and processing within 10 ms. Notably, the algorithm that was implemented based on FPGA not only provides the  $n$ – $\gamma$  discrimination accuracy of 99.1% with a FOM of 1.30, but also gives an intrinsic timing error of less than 135 ps. The neutron transport simulation conducted by using Geant4 shows the reasonable distribution of the flight time spectrums and presents the flight time spectrum for 2.45 MeV neutrons with the peak value of 92 ns. The obtained results prove that the TOFII spectrometer will be able to provide neutron information at HL-2M, and the future work mainly includes the calibration experiment of the TOFII by using mono-energetic neutron sources. After the system calibration and the completion of HL-2M construction, the TOFII spectrometer system will be used to achieve NES diagnosis at HL-2M.

## References

1. M.G. Johnson, L. Giacomelli, A. Hjalmarsson et al., The 2.5-MeV neutron time-of-flight spectrometer TOFOR for experiments at JET. *Nucl. Instrum. Methods A* **591**, 417–430 (2008). <https://doi.org/10.1016/j.nima.2008.03.010>
2. Y. Shibata, T. Iguchi, Time-of-flight neutron spectrometer for JT-60U. *Rev. Sci. Instrum.* **72**, 828 (2001). <https://doi.org/10.1063/1.1323240>
3. A. Hjalmarsson, S. Conroy, G. Ericsson et al., The TOFOR spectrometer for 2.5 MeV neutron measurements at JET. *Rev. Sci. Instrum.* **74**, 1750 (2003). <https://doi.org/10.1063/1.1534401>
4. C. Guerrero, A. Tsinganis, E. Berthoumieux et al., Performance of the neutron time-of-flight facility n TOF at CERN. *Eur. Phys. J. A* **49**, 27 (2013). <https://doi.org/10.1140/epja/i2013-13027-6>
5. X. Zhang, J. Källne, G. Gorini et al., Second generation fusion neutron time-of-flight spectrometer at optimized rate for fully digital data acquisition. *Rev. Sci. Instrum.* **85**, 043503 (2014). <https://doi.org/10.1063/1.4869804>
6. W. Zhang, T. Wu, B. Zheng et al., A real-time neutron–gamma discriminator based on the support vector machine method for the time-of-flight neutron spectrometer. *Plasma Sci. Technol.* **20**, 045601 (2018). <https://doi.org/10.1088/2058-6272/aaaa9>
7. Q. Li, The component development status of HL-2M tokamak. *Fusion Eng. Des.* **82**, 561–566 (2007). <https://doi.org/10.1016/j.fusengdes.2015.06.106>
8. D.Q. Liu, H. Ran, G.S. Li et al., Engineering design for the HL-2M tokamak components. *Fusion Eng. Des.* **88**, 679–682 (2013). <https://doi.org/10.1016/j.fusengdes.2013.04.035>
9. D. Liu, T. Lin, T. Qiao et al., Assembly study for HL-2M tokamak. *Fusion Eng. Des.* **96–97**, 298–301 (2015). <https://doi.org/10.1016/j.fusengdes.2015.06.026>
10. D. Liu, C. Zhou, Z. Cao et al., Construction of the HL-2A tokamak. *Fusion Eng. Des.* **66–68**, 147 (2003). [https://doi.org/10.1016/S0920-3796\(03\)00165-0](https://doi.org/10.1016/S0920-3796(03)00165-0)
11. Q. Li, Brief introduction to engineering and experiment of HL-2A tokamak. *At. Energy Sci. Technol.* **43**, 204 (2009). (in Chinese)
12. Y. Liu, X. Ding, Q. Yang et al., Recent advances in the HL-2A tokamak experiments. *Nucl. Fusion* **45**, S239–S244 (2005). <https://doi.org/10.1088/0029-5515/45/10/S19>
13. G.C. Neilson, D.B. James, Time of flight spectrometer for fast neutrons. *Rev. Sci. Instrum.* **26**, 1018 (1955). <https://doi.org/10.1063/1.1715178>
14. G.J.F. Legge, P. Van der Merwe, A double scatter neutron spectrometer. *Nucl. Instrum. Methods* **63**, 157–165 (1968). [https://doi.org/10.1016/0029-554X\(68\)90321-2](https://doi.org/10.1016/0029-554X(68)90321-2)
15. G. Gorini, J. Källne, High count rate time-of-flight spectrometer for DD fusion neutrons. *Rev. Sci. Instrum.* **63**, 4548 (1992). <https://doi.org/10.1063/1.1143663>
16. S. Agostinelli, J. Allison, K. Amako et al., Geant4: a simulation toolkit. *Nucl. Instrum. Methods A* **506**, 250–303 (2003). [https://doi.org/10.1016/S0168-9002\(03\)01368-8](https://doi.org/10.1016/S0168-9002(03)01368-8)
17. Q. Tang, Z. Zhao, M. Su et al., Performance calculation of ultra fast neutron scintillator. *High Power Laser Part. Beams* **22**, 1243 (2010). <https://doi.org/10.3788/HPLPB20102206.1243>. (in Chinese)
18. H. Liu, Development and application of the PXI technology. *Meas. Control Technol.* **25**, 51–53 (2006). <https://doi.org/10.1007/s10614-006-9021-y>. (in Chinese)
19. J. Christiansen, HPTDC high performance time to digital converter version 2.1 CERN/EP-MIC, CERN, Geneva (2002). <http://cds.cern.ch/record/1067476>
20. W. Fan, B. Zheng, J. Cao et al., Development of a fast electron bremsstrahlung diagnostic system based on LYSO and silicon photomultipliers during lower hybrid current drive for tokamak. *Plasma Sci. Technol.* **21**, 065104 (2019). <https://doi.org/10.1088/2058-6272/ab0a77>
21. M.G. Johnson, S. Conroy, M. Cecconello et al., Modelling and TOFOR measurements of scattered neutrons at JET. *Plasma Phys. Control. Fusion* **52**, 085002 (2010). <https://doi.org/10.1088/0741-3335/52/8/085002>
22. S.A. Pozzi, M.M. Bourne, S.D. Clarke, Pulse shape discrimination in the plastic scintillator EJ-299-33. *Nucl. Instrum. Methods A* **723**, 19–23 (2013). <https://doi.org/10.1016/j.nima.2013.04.085>

23. E.V. Pagano, M.B. Chatterjee, E. De Filippo et al., Pulse shape discrimination of plastic scintillator EJ 299-33 with radioactive sources. *Nucl. Instrum. Methods A* **889**, 83–88 (2018). <https://doi.org/10.1016/j.nima.2018.02.010>
24. M.J. Joyce, M.D. Aspinall, F.D. Cave et al., The design, build and test of a digital analyzer for mixed radiation fields. *IEEE Trans. Nucl. Sci.* **57**, 2625–2630 (2010). <https://doi.org/10.1109/TNS.2010.2044245>
25. M.D. Aspinalla, B. D’Mellowa, R.O. Mackina et al., The empirical characterization of organic liquid scintillation detectors by the normalized average of digitized pulse shapes. *Nucl. Instrum. Methods A* **578**, 261–266 (2007). <https://doi.org/10.1016/j.nima.2007.05.114>
26. V. Vapnik, *Estimation of Dependences Based on Empirical Data* (Springer, New York, 2006). <https://doi.org/10.1007/0-387-34239-7>
27. C. Cortes, V. Vapnik, Support-vector networks. *Mach. Learn.* **20**, 273–297 (1995). <https://doi.org/10.1007/BF00994018>
28. C.J.C. Burges, A tutorial on support vector machines for pattern recognition. *Data Min. Knowl. Discov.* **2**, 121–167 (1998). <https://doi.org/10.1023/A:1009715923555>
29. S. Liu, C. Feng, Q. An et al., BES III time-of-flight readout system. *IEEE Trans. Nucl. Sci.* **57**, 419–427 (2010). <https://doi.org/10.1109/TNS.2009.2034520>
30. G.S. Gao, R. Partridge, High speed digital TDC for D0 vertex reconstruction. *IEEE Trans. Nucl. Sci.* **38**, 286–289 (1991). <https://doi.org/10.1109/23.289311>
31. Z. Kohley, E. Lunderberg, P.A. DeYoung et al., Modeling interactions of intermediate-energy neutrons in a plastic scintillator array with GEANT4. *Nucl. Instrum. Methods A* **682**, 59–65 (2012). <https://doi.org/10.1016/j.nima.2012.04.060>
32. S.F. Naeem, S.D. Clarke, S.A. Pozzi, Validation of Geant4 and MCNPX-PoliMi simulations of fast neutron detection with the EJ-309 liquid scintillator. *Nucl. Instrum. Methods A.* **714**, 98–104 (2013). <https://doi.org/10.1016/j.nima.2013.02.017>